Investigation of Beamforming Patterns from Volumetrically Distributed Phased Arrays

Drew Overturf[1], Kris Buchanan[1], Jeff Jensen[2], Carlos Flores-Molina[1], Sara Wheeland[1], and Gregory H. Huff[2]

[1]Space and Naval Warfare Systems Center Pacific (SSC–Pacific), San Diego, CA 92152-5001

[2]Dept. of Electrical and Computer Engineering, Texas A&M University, College Station, TX 77843

***Abstract*— This work presents distributed beamforming using three dimensional randomly distributed volumetric arrays. This work examines a statistical ensemble (mean-valued) of average beampattern behavior for canonical and non-canonical volumetrically bound distributed (random) antenna arrays. Cubical, cylindrical, and spherical topologies of isotropic elements are analyzed to show beamforming and scanning from zenith to meridian for canonical topologies. In addition, small amounts of work have previously been investigated and therefore this work helps to enlighten with illustrations of the beampattern phenomena of a select few non-conically bound distributed and volumetric structures. To validate the distributed array pattern behavior, the manifold is composed of one million isotropic radiators densely populated amongst geometrical bounds to examine characteristic pattern behavior. This provides faithful convergence of numerical beampatterns to their expected (mean) patterns. Last of all, results show an increasing complexity of pattern behavior for use in many spatial advancements in distributed beamforming.**

***Index Terms*— Antenna arrays; collaborative beamforming; distributed beamforming; phased arrays; random arrays.**

I. Introduction

INCREASED interest exists for larger apertures which require higher throughput and higher bandwidth. As such, multiple antennas have to be adapted to meet growing system demands. Since many practical scenarios limit precise element placement, a volumetric aperture helps to alleviate these concerns by providing a third degree of freedom in the design space. Furthermore, this third degree of freedom is seen to advance the problem space of antenna array and distributed beamforming design with greater flexibility in pattern behavior and element synchronization concerns. In this paper, we present an analysis of various volumetric array topologies to examine the statistical pattern behavior. We consider three dimensional models useful in advancements of wireless aerial networks and other scenarios of mobile and volumetric architectures.

Modern wireless technologies, such as ad-hoc networking, require agile and controllable antennas on their frontends. These networks often require wide bandwidth, high directivity, and pattern stability. To that end, individual antennas are combined into a larger aperture phased array. Traditionally, these antennas are designed as periodic structures, where each element is placed in a lattice. The elements constructively add in-phase to achieve main beam steer-ability and improved directivity. However, periodic arrays suffer from problems such as scan blindness, surface-wave formation, and tight fabrication constraints [1-6]. Randomly and/or sparsely distributing the elements alleviates these issues while also considerably increasing the bandwidth of pattern stability [2]. In contrast to deterministic arrays, the analysis and design of random arrays require the use of probabilistic methods. The array factor is best characterized by determining its expected (mean) value over a given distribution. Mathematically, the general expression for a 3D array is [1-2]:

$$F\left(\theta,\phi\middle|\mathrm{x}_n,\mathrm{y}_n,\mathrm{z}_n\right)=\frac{1}{N}\sum_{n=1}^{N}e^{j(uX+vY+wZ)} \tag{1}$$

$$X=\tilde{r}_n\sin\theta_n\cos\phi_n, Y=\tilde{r}_n\sin\theta_n\sin\phi_n, Z=\tilde{r}_n\cos\theta_n,$$
$$\mathrm{X}\triangleq\left\langle \mathrm{X},\mathrm{Y},\mathrm{Z}\right\rangle,\ -1\le \mathrm{X}\le 1, \tilde{r}_n=r_n/A, \tilde{A}=A/\lambda$$
$$u=\zeta_x^r\left(\theta,\phi\right)=kA\,\hat{\mathrm{x}}\cdot\left(\hat{\mathrm{r}}\left(\theta,\phi\right)-\hat{\mathrm{r}}\left(\theta_0,\phi_0\right)\right), \tag{2}$$
$$v=\zeta_y^r\left(\theta,\phi\right)=kA\,\hat{y}\cdot\left(\hat{\mathrm{r}}\left(\theta,\phi\right)-\hat{\mathrm{r}}\left(\theta_0,\phi_0\right)\right),$$
$$w=\zeta_z^r\left(\theta\right)=kA\,\hat{z}\cdot\left(\hat{\mathrm{r}}\left(\theta,\phi\right)-\hat{\mathrm{r}}\left(\theta_0,\phi_0\right)\right), \sqrt{u^2+v^2+w^2}=1$$

When discussing random arrays, the mean beampattern for any geometrically-bound topology can improve relative radiative characteristics. This process has been shown in [1-2] by taking the expected value of the power pattern $|\bar{F}(\Psi)^2|$ across the unit interval [-1, 1]. For a volumetric random variable *x*, this provides a general theory towards obtaining the characteristic functions of (3) which are orthogonal in all three axes and uncorrelated:

$$\bar{U}=\frac{1}{N}+\left(1-\frac{1}{N}\right)\Lambda|u|^2\,\Lambda|v|^2\,\Lambda|w|^2=\frac{1}{N}+\left(1-\frac{1}{N}\right)\Lambda\left|\vec{\Psi}\right|^2,$$
$$\Lambda\left|\vec{\Psi}\right|^2=\left|\Lambda\left(\zeta_x^r\left(\theta,\phi\right)\right)\Lambda\left(\zeta_y^r\left(\theta,\phi\right)\right)\Lambda\left(\zeta_z^r\left(\theta\right)\right)\right|^2,=\mathcal{F}\left\{\mathrm{PDF}\right\}, \tag{3}$$
$$\Psi=kA\left(\hat{\mathrm{r}}\left(\theta,\phi\right)-\hat{\mathrm{r}}\left(\theta_0,\phi_0\right)\right)=\cos^{-1}\left[u\quad v\quad w\right],$$

Here, the first term, $1/N$ is a pedestal which describes the average value in the sidelobe region, while the second term describes the shape of the main beam. The Λ functions inside the square magnitude are 1D characteristic functions of the probability distributions (PDF) that govern the randomness within a specified geometry. Similar to standard array theory, the total main beam factor is given by the product of

978-1-5386-0595-0/17/$31.00 ©2017 IEEE

characteristic functions in each coordinate axis *x*, *y*, and *z*. This is done by evaluating the functions in terms of the directional cosine steering vectors $\zeta_x^r(\theta, \phi)$. As characteristic functions are Fourier transforms of the corresponding PDFs, they provide an alternative means to describing a distribution. This connection relates directly to the well-known Fourier transform relations for aperture antennas and arrays [2-5].

II. Analysis of Random Array Topologies

The probability density function of a uniformly distributed circular canonical family (4) is derived from the joint density function of (5) and renormalized by (6) such that dimensional topology increases by the order of *n*. As an example, the ring, line, circle and spherical geometrical distributions are generated by substitution of *n=0*, 1, 2, and 3 respectively. An illustration is provided in Fig 1 along with it's cumulative density function of (7).

$$f_X(x) = \left((1-x^2)\Gamma(5/2+n)\right) \Big/ \left(\sqrt{\pi}\Gamma\left((1+n)/2\right)\right) \tag{4}$$

$$\int_{-\sqrt{1-y^2-z^2}}^{\sqrt{1-y^2-z^2}} \int_{-\sqrt{1-y^2}}^{\sqrt{1-y^2}} \int_{-1}^{1} f_{X,Y,Z}(x,y,z)\left(\sqrt{1-x^2-y^2-z^2}\right)^n dxdydz = 1 \tag{5}$$

$$\Rightarrow f_{X,Y,Z}(x,y,z)\big|_{A=1} = \left((1+n)\Gamma(5/2+n)\right) \Big/ \left(\pi^{3/2}\Gamma(2+n)\right)$$

$$f_E(x;n) = \frac{\left(1-x^2\right)^{\frac{n-1}{2}}\Gamma(1+n/2)}{\sqrt{\pi}\Gamma\left((n+1)/2\right)} \quad \neg(n \geq -1) \quad \textit{Even Distribution} \tag{6}$$

$$f_O(x;n) = f_E(x;n)\,\mathrm{sgn}(x) \quad \neg(n \geq -1) \quad \textit{Odd Distribution}$$

$$F_X(x) = \frac{2x\Gamma(1+n/2)\,{}_2F_1\left(1/2,(1-n)/2;3/2;x^2\right)}{\sqrt{\pi}\Gamma\left((1+n)/2\right)} \tag{7}$$

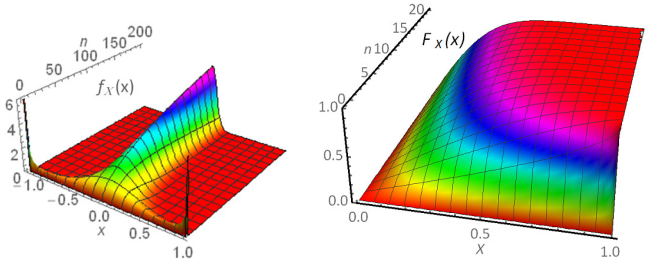

Fig 1. PDF-left and CDF-right of a circularly distributed element population.

Examples of mean-valued beam patterns are illustrated in Fig 2 for a spherical random array (*SRA, n=3*), a circular random array (*CRA, n=2*), a ring random array (*RRA*, *n* = 0), and a linear random array, (*LRA*, *n = 1*). These cases show the spatial variations of the effective aperture ($\tilde{A} = A/\lambda$) and pattern variation outside of the circularly symmetric Psi space:

$$\bar{U}(\theta,\phi) \overset{Sph}{=} \begin{matrix} 1/N + (1-1/N)3^3 \\ \neg\,\mathrm{tinc}(x) = j_1(x)/x \end{matrix} \left[\left|\mathrm{tinc}\,u\right|^2 \left|\mathrm{tinc}\,v\right|^2 \left|\mathrm{tinc}\,w\right|^2\right] \tag{8}$$

$$\bar{U}(\theta,\phi) \overset{Cir}{=} \begin{matrix} 1/N + (1-1/N)2^2 \\ \neg\,\mathrm{jinc}(x) = J_1(x)/x \end{matrix} \left[\left|\mathrm{jinc}(u)\right|^2 \left|\mathrm{jinc}(v)\right|^2\right] \tag{9}$$

$$\bar{U}(\theta,\phi) \overset{Ring}{=} \begin{matrix} 1/N + (1-1/N) \\ \neg\,\mathrm{rinc}(x) = J_0(x) \end{matrix} \left[\left|\mathrm{rinc}(u)\right|^2 \left|\mathrm{rinc}(v)\right|^2\right] \tag{10}$$

$$\bar{U}(\theta,\phi) \overset{Line}{=} \begin{matrix} 1/N + (1-1/N) \\ \neg\,\mathrm{sinc}(x) = j_0(x) \end{matrix} \left[\left|\mathrm{sinc}(u)\right|^2\right] \tag{11}$$

$$\Lambda_E(\Psi;n) = \int_{-1}^{1} f_E(x;n) e^{jx\Psi} = \mathrm{Sinc}_n(\Psi)$$
$$\neg\mathrm{Sinc}(\Psi;n) = \Gamma(n/2+1)J_{n/2}(\Psi)/(\Psi/2)^{n/2} \tag{12}$$

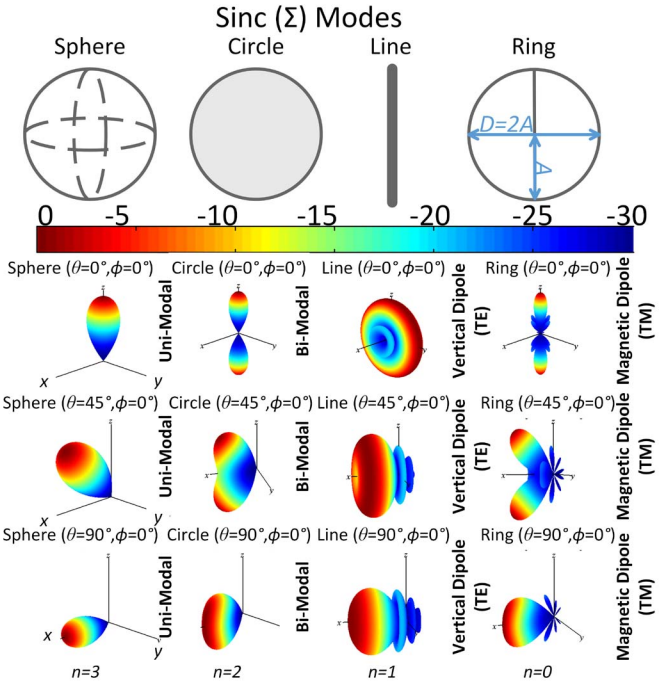

Fig 2. Beampatterns *n*=0-4 of the Sinc_n modes of (12).

III. System Model

Here we present an investigation of volumetrically distributed random antenna arrays. Such arrays can be formed ad-hoc from distributed wireless sensors, similar to swarms found in nature. To model this type of morphing array behavior, we analyze a cube, a cylinder, and a sphere as the bounding structure. Arrays are classically 2D structures, either linear or planar; however, volumetric array patterns do not suffer from alias beams. This prevents unrecoverable energy loss. The application of these three topologies to the mean array factor (3) yields three sets of characteristics functions, Λ_{cube}, $\Lambda_{\mathrm{cylinder}}$, and $\Lambda_{\mathrm{sphere}}$:

$$\Lambda_{cube}(\theta,\phi) = \left[\left|\mathrm{sinc}\,\zeta_x^r\right|^2 \left|\mathrm{sinc}\,\zeta_y^r\right|^2 \left|\mathrm{sinc}\,\zeta_z^r\right|^2\right]$$
$$\Lambda_{cube}(u,v,w) = \left[\left|\mathrm{sinc}\,u\right|^2 \left|\mathrm{sinc}\,v\right|^2 \left|\mathrm{sinc}\,w\right|^2\right] \tag{13}$$

$$\Lambda_{cylinder}(\theta,\phi) = \left[\left|\mathrm{jinc}\,\zeta_x^r\right|^2 \left|\mathrm{jinc}\,\zeta_y^r\right|^2 \left|\mathrm{sinc}\,\zeta_z^r\right|^2\right]$$
$$\Lambda_{cylinder}(u,v,w) = \left[\left|\mathrm{jinc}\sqrt{u^2+v^2}\right|^2 \left|\mathrm{sinc}\,w\right|^2\right] \tag{14}$$

$$\Lambda_{sphere}(\theta,\phi)=\left[\left|\text{tinc}\,\zeta_x^r\right|^2\left|\text{tinc}\,\zeta_y^r\right|^2\left|\text{tinc}\,\zeta_z^r\right|^2\right]$$
$$\Lambda_{sphere}(\text{u},\text{v},\text{w})=\left[\left|\text{tinc}\sqrt{u^2+v^2+w^2}\right|^2\right] \quad (15)$$

where the (θ, ϕ) dependence is suppressed for notation simplicity. Here, *jinc* and *tinc* are extensions of *sinc* where the *sin* function becomes a Bessel function J_n and spherical Bessel function j_n, respectively. In the next section, we present preliminary numerical analysis of the cube, cylinder, and spherical array factor.

IV. Simulated Results

Numerical simulation by direct integration of three topologies with $N = 10^6$ isotropic elements calculated the radiation patterns. The elements were uniformly distributed within the volumetric bounds of a cube, cylinder, and sphere. Amplitude tapering is not applied to isolate the effect of geometry. Fig 3 - Fig 5 shows the topographical *UV* and angular (θ, ϕ) patterns with meridian and zenith scans for the cube, sphere and cylinder arrays. Sharp edges on the cubic and cylindrical distributions contribute to peaking sidelobes around the main beam. As the cube smooths to a cylinder then to a sphere, diffraction effects diminish as the edges disappear. This is similar to ray-tracing in that the scattering divergence is minimized from sharp corners.

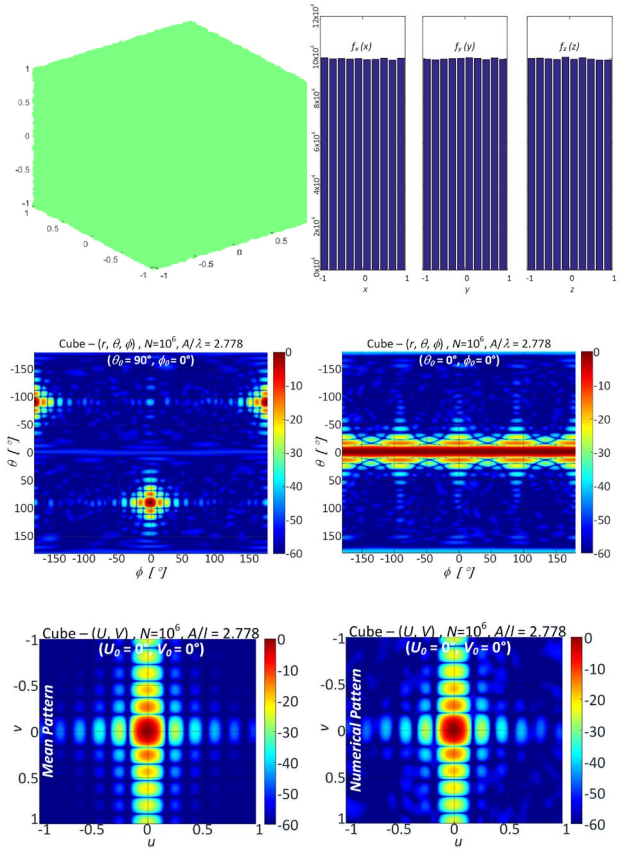

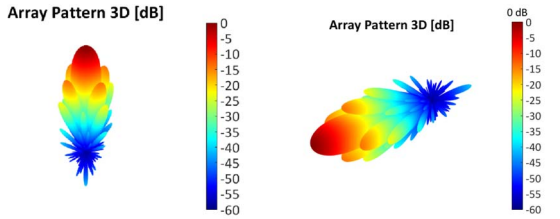

Fig 3. Model (left) and numerical (right) results; cube-array.

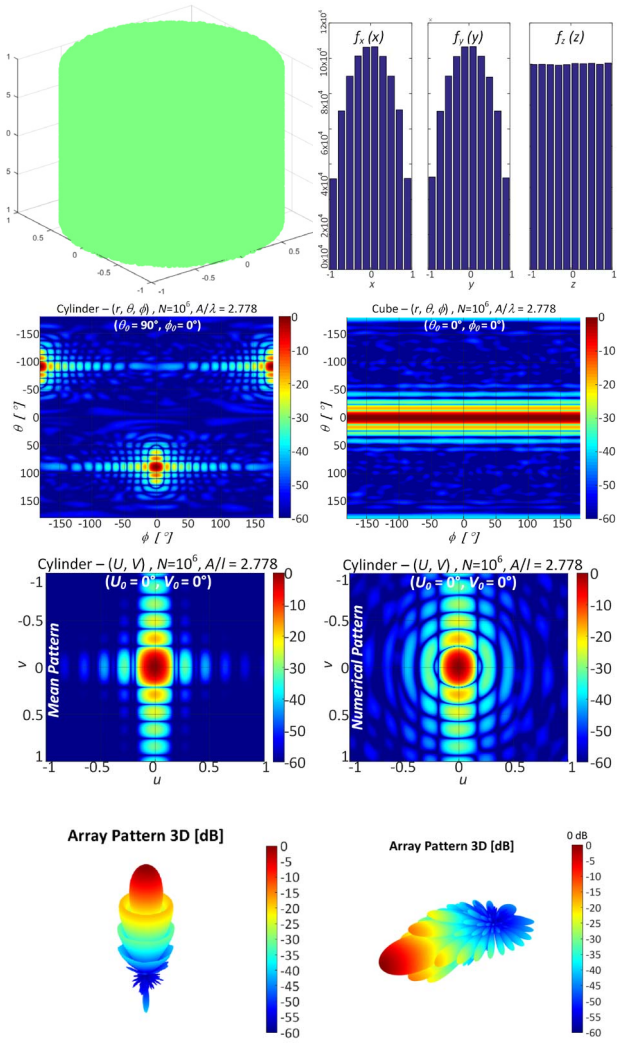

Fig 4. Model (left) and numerical (right) results; cylinder-array.

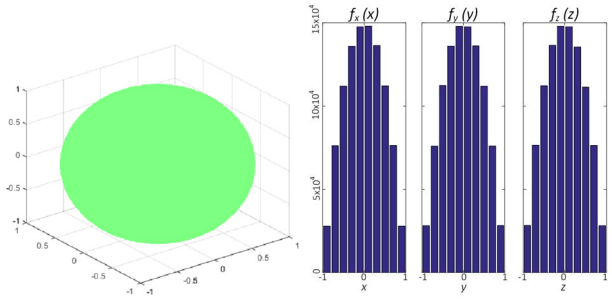

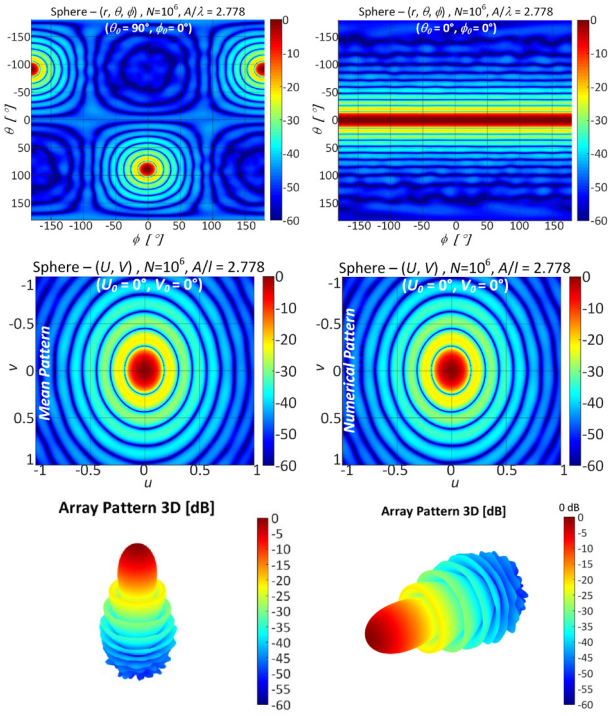

Fig 5. Model (left) and numerical (right) results; spherical array.

V. Hollow Volumetric Cubical, Cylindrical and Spherical Arrays

The characteristic function representations of the hollow volumetric cube, cylinder, and sphere (shell) are given by (16) – (18), respectively. The shell does not contain a line fill. A line n=1 fills a circle n=2, and then a sphere n=3; whereas a ring n=0 is the perimeter of the planar n=2 and volumetric n=3 modes. Additionally, the ring is a 1-sphere and the line is a 1-ball. A convolution of the ring fills the line without touching the perimeter and makes a 2-ball with a 1-sphere boundary. This extends to 3D space with a 2-sphere boundary and 3-ball filling. A convolution deletes the inside of the sphere, but preserves the boundary. A final comparison of the beampatterns of (16) – (18) is illustrated in Fig 6 – Fig 7.

$$\Lambda_{Hollow\ Cube}(\theta,\phi)=\left[\left|\begin{pmatrix}\operatorname{sinc}\zeta_x^r\operatorname{sinc}\zeta_y^r\operatorname{sinc}\zeta_z^r\end{pmatrix}\right|^2\right]$$
$$\begin{pmatrix}\cos\zeta_x^r+\cos\zeta_y^r+\cos\zeta_z^r\end{pmatrix}\Bigg|\Bigg] \quad (16)$$

$$\Lambda_{Hollow\ Cube}(\mathrm{u},\mathrm{v},\mathrm{w})=\left[\left|\begin{pmatrix}\operatorname{sinc}u\operatorname{sinc}v\operatorname{sinc}w\end{pmatrix}\right|^2\right]$$
$$\begin{pmatrix}\cos u+\cos v+\cos w\end{pmatrix}\Bigg|\Bigg]$$

$$\Lambda_{Hollow\,Cylinder}(\theta,\phi)=\left[\left|\operatorname{rinc}\zeta_x^r\right|^2\left|\operatorname{rinc}\zeta_x^r\right|^2\left|\operatorname{sinc}\zeta_x^r\right|^2\right] \quad (17)$$

$$\Lambda_{Hollow\,Cylinder}(\mathrm{u},\mathrm{v},\mathrm{w})=\left[\left|\operatorname{rinc}\sqrt{u^2+v^2}\right|^2\left|\operatorname{sinc}w\right|^2\right]$$

$$\Lambda_{shell}(\theta,\phi)=\left[\left|\operatorname{tinc}\zeta_x^r\right|^2\left|\operatorname{tinc}\zeta_x^r\right|^2\left|\operatorname{shinc}\zeta_z^r\right|^2\right]$$

$$\Lambda_{shell}(\mathrm{u},\mathrm{v},\mathrm{w})=\left[\left|\operatorname{tinc}\sqrt{u^2+v^2}\right|^2\left|\operatorname{shinc}w\right|^2\right] \quad (18)$$

$$\neg\operatorname{shinc}(x)=3\left(\operatorname{sinc}(x)-\operatorname{tinc}(x)\right)/2$$

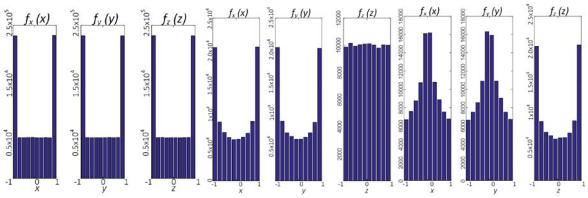

Fig 6. Hollow cube – left, cylinder – middle; shell – right.

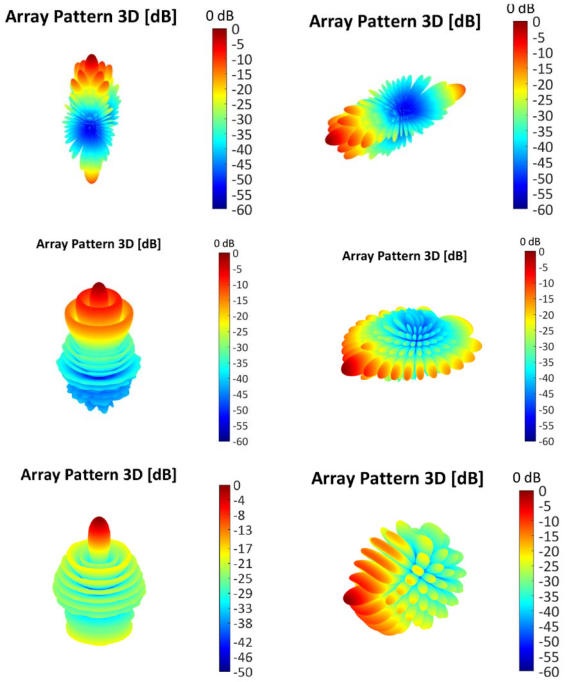

Fig 7. Beampatterns of hollow cube (top), cylinder (middle) and shell (bottom) steered zenith (left) to meridian (right).

VI. Non-Canonical Distributions

Simulations of a hyperboloid of two sheets, hyperboloid of one sheet, cone and psuedosphere volumetric arrays were performed to compare their resultant patterns. In all cases, the number of elements was set to $N = 10^6$ to accurately model the limiting sidelobe patterns; the effective aperture was set to be A/λ = 5.5 for the hyperboloids and A/λ =2.6215 for the cone and psuedosphere as illustrated in Fig 8. 3D patterns are extracted and scanned to meridian (xy-plane) relative to the xy plane.

Observation of Fig 8 illustrates that the hyperboloids provide narrower beamwidths. In addition, the hyperboloid of one sheet is shown to have a deep null when scanned at the meridian whereas the hyperboloid of two sheets provides higher sidelobe behavior.

The cone and psuedosphere have larger beamwidths compared to the hyperboloids, due their smaller aperture size. The meridian scan plane of the cone also provides limited sidelobe activity and is much different than that of the psuedosphere with higher sidelobe activity.

The psudeosphere indicates symmetrical sidelobe behavior tapering downward in its elevation plane. Lastly, the pseudosphere with a large backlobe is indicative of its small elevational aperture size and is similar to alias beams found in planar geometries.

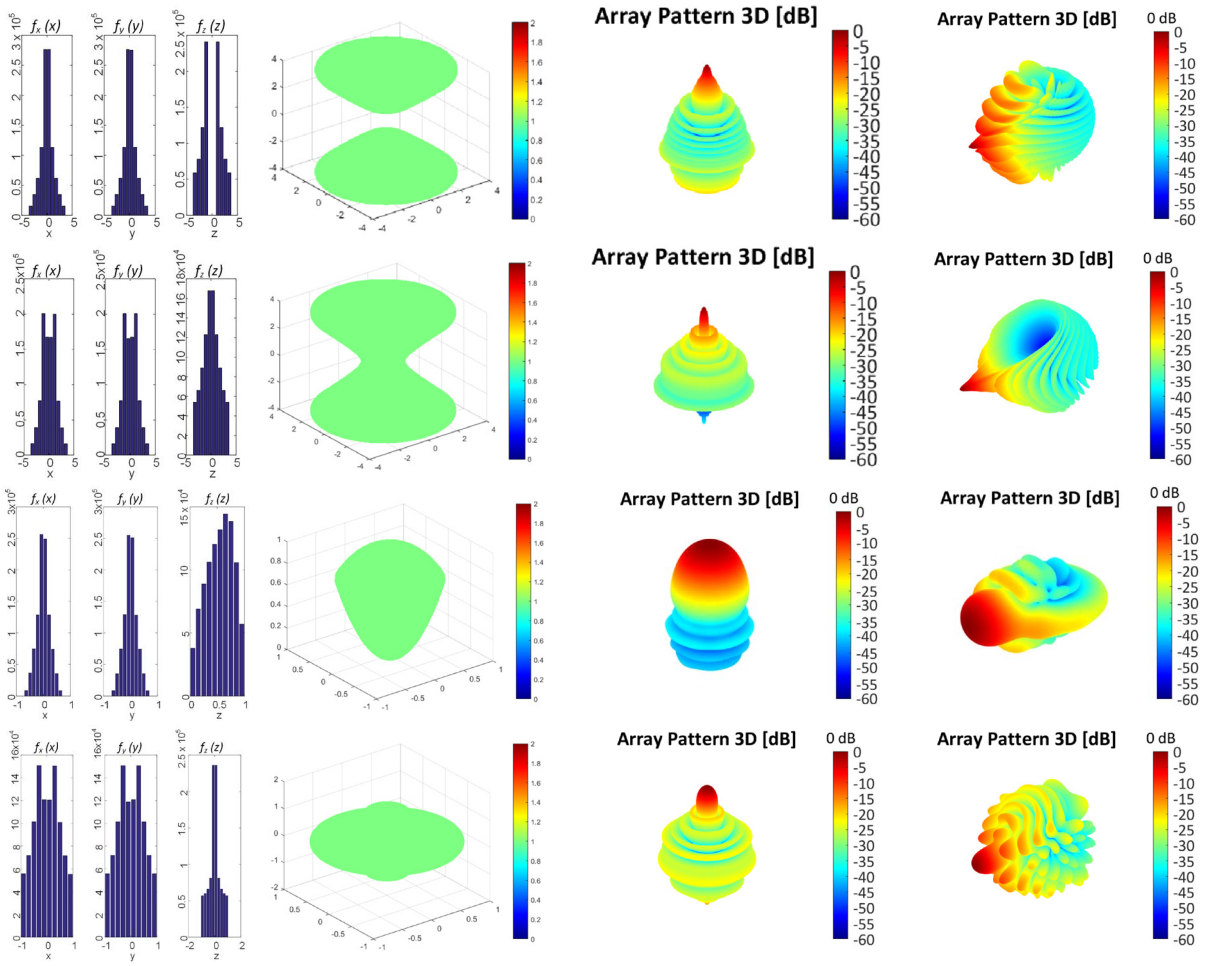

Fig 8. Simulated results of four non-canonical volumetric topologies densely packed and scanned from the zenith to the meridian elevation.

VII. Experimental Results

A. *Madam "Medusa": a Polymorphic Phased Array Distribution*

Simulated and experimental results (Fig 9 - Fig 10, respectively) were obtained for the cube, cylinder and sphere random arrays, each confined to a geometry of radius A = 34 cm. The antenna elements used in each array are quarterwave monopoles operating in the 2.4 GHz ISM band with an approximately uniform radiation pattern in the azimuth plane. In order to maintain a constant aperture size, the number of elements for each array topology varies due to size constraints on the antennas. A modular controller (Fig 10) and smartphone application were used in this work to steer a single main beam at the meridian elevation angle (meridian – location, $\theta_0 = 90°$, $\phi_0 = 0°$) and in the $\phi = 0°$ azimuth plane. A rotated patch element distribution was also experimentally validated in order to observe fluctuations of pattern behavior, which were still seen to obey trends of the characteristic pedestal of $1/N \approx$ -16 dB down from the mainbeam.

B. *The Shell Distribution*

Experimental and simulated validation of the shell is provided in Fig 12 for comparison of a hollow three dimensional array structure. From well-known electromagnetic theory, a current loop is a lower order mode than that of a linear electric source. Hence, it becomes apparent why the hollow sphere (shell) is a mode in between the line and the ring as provided in Fig 12. The characteristic function of the shell is given by (18) with respective element distribution in (19). In other words, the shell does not contain the filling of a line and has a parabolic distribution (i.e. diverging distributional behavior similar to the jinc modes). Simulated scan behavior at the meridian elevation angle is provided in Fig 13 along with comparisons to measured results and its characteristic solution in Fig 14 .

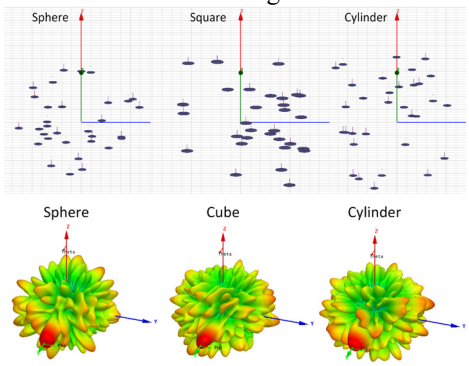

Fig 9. Simulated scan behavior of a sphere, cube and cylinder.

$$3/2\left(\text{tinc}\left(\Psi\right)-\text{sinc}\left(\Psi\right)\right) \quad (18)$$

$$f_X\left(x\right)=3/8\left(1+x^2\right) \quad (19)$$

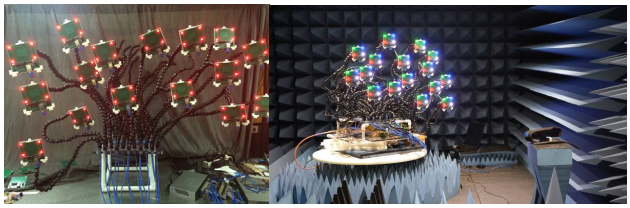

Fig 10. Volumetric array test setup

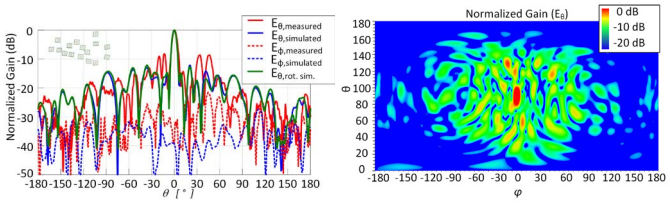

Fig 11. Simulated rotated patch element distribution shown in the top left.

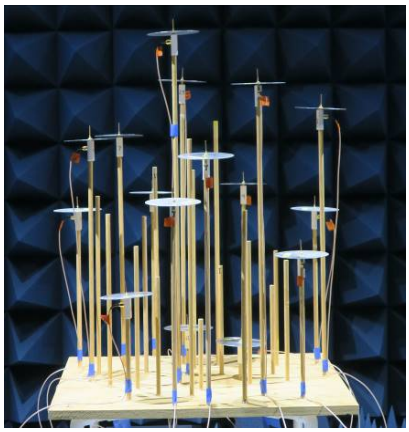

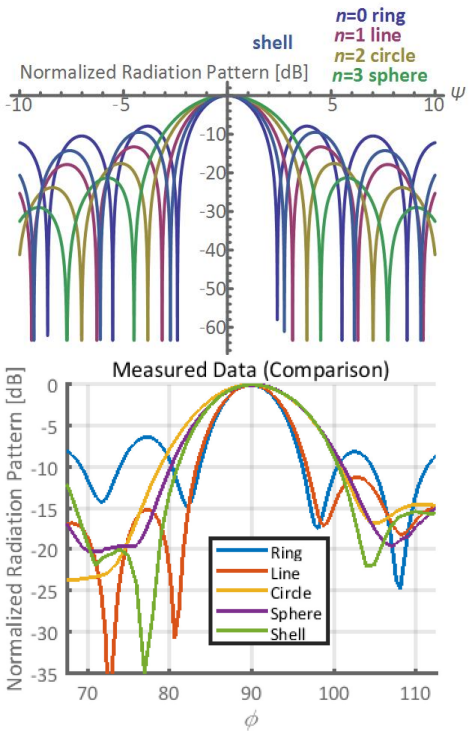

Fig 12. Comparison of the ring, shell, line, circle and sphere; theoretical-top, measured-bottom, A/λ=2.778.

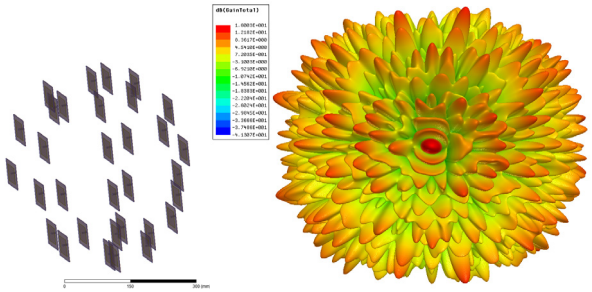

Fig 13. 32 patch element Shell Distribution, A/λ=6.

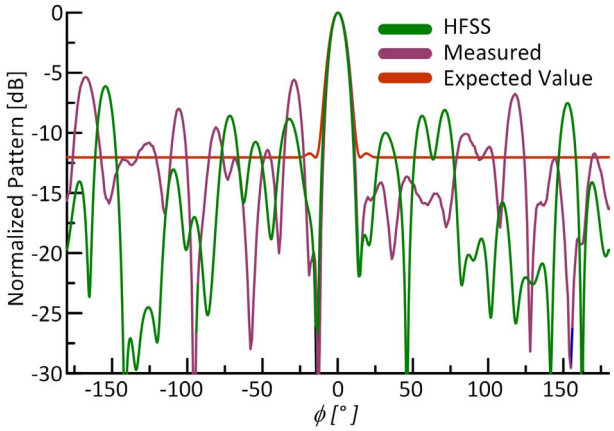

Fig 14. Comparison of the simulated, measured and closed form solutions for a uniformly distributed shell array.

VIII. CONCLUSION

This work studied beampatterns from both canonical and non-canonical configurations of geometrically bound distributed array topologies. In our analysis, we found that the radiation patterns from smaller volumes produce larger pattern widths whereas topologies with larger volumes produce narrower patterns agreeing with previous works of [1-6]. Future works should look at comparisons between conical volumetric topologies against their non-canonical counterparts. Other works may compare patterns stemming from positive and negative curvatures.

REFERENCES

[1] K. Buchanan and G. Huff, "A Stochastic Mathematical Framework for the Analysis of Spherically Bound Random Arrays," *IEEE Trans. Antennas Propag.*, vol. 62, pp. 3002-3011, June 2014.

[2] K. R. Buchanan, "Theory and Applications of Aperiodic (Random) Phased Arrays," Ph.D. dissertation, Dept. Elect. & Com. Eng., Texas A&M University, TX, Aug. 2014.

[3] H. Ochiai, "Collaborative beamforming for distributed wireless ad hoc sensor networks," *IEEE Trans. Signal Process.*, vol. 53, pp. 4110, Nov. 2005.

[4] Y. Lo, "A probabilistic approach to the design of large antenna arrays," *IEEE Trans. Antennas Propag.*, vol. 11, pp. 95-96, Jan. 1963.

[5] T. A. Dzekov and R. S. Berkowitz, "Parameters of a spherical random antenna array," *Electronics Lett.*, vol. 14, pp. 495-496, Aug 1978.

[6] B. D. Steinberg, Principles of Aperture & Array System Design, New York: Wiley, 1976.